FEBS Letters 582 (2008) 1437–1443

Dynamics of Cdc42 network embodies a Turing-type mechanism of yeast cell polarity

Andrew B. Goryachev*, Alexandra V. Pokhilko

Centre for Systems Biology at Edinburgh, School of Biological Sciences, University of Edinburgh, Edinburgh EH9 3JR, United Kingdom

Received 18 March 2008; accepted 19 March 2008

Available online 31 March 2008

Edited by Felix Wieland

A.B.G. dedicates this work to his parents and D.S. Chernavskii

Abstract **Complex biochemical networks can be understood by identifying their principal regulatory motifs and mode of action. We model the early phase of budding yeast cellular polarization and show that the biochemical processes in the presumptive bud site comprise a Turing-type mechanism. The roles of the prototypical activator and substrate are played by GTPase Cdc42 in its active and inactive states, respectively. We demonstrate that the nucleotide cycling of Cdc42 converts cellular energy into a stable cluster of activated Cdc42. This energy drives a continuous membrane-cytoplasmic exchange of the cluster components to counteract diffusive spread of the cluster. This exchange explains why only one bud forms per cell cycle, because the winner-takes-all competition of candidate sites inevitably selects a single site.**

Keywords: Cell polarity; Small GTPases; Self-organization; Network motifs; Turing model; Budding yeast

1. Introduction

Emergence of cellular polarity is a symmetry-breaking event through which a cell acquires an internal structural and functional axis. This is vitally important for the cell to migrate or grow along morphogen gradients, select a direction for division, and transmit neural information [1,2]. The transition from a functionally symmetric to a polarized form is an example of pattern formation manifested by many self-organizing systems [3]. Following the pioneering work of A. Turing [4], various models of the activator–inhibitor type have been suggested to explain the spontaneous emergence of cellular polarity [5–8]. However, the specific molecular mechanisms that fit the requirements of the Turing model have been largely elusive [9] and, therefore, the applicability of the Turing theory to these systems has not been demonstrated unambiguously. Here we provide a detailed analysis of the experimentally determined molecular network that is responsible for the early phase of yeast bud formation, a prototypical example of cellular polarization [10]. We demonstrate that the molecular interactions between the small Rho GTPase Cdc42, its regulatory molecules and its effector Bem1 are sufficient to explain the spontaneous emergence of a unique yeast bud. We show that the core biochemical mechanism of this phenomenon can be described by a prototypical Turing-type model.

Importantly, we find that the polarization mechanism is fundamentally dependent on the switch-like property of small GTPases. These essential proteins normally exist in two alternative conformations: the active, when bound to a molecule of guanosine triphosphate (GTP), and the inactive, when associated with guanosine diphosphate (GDP) [1]. While in vitro small GTPases are capable of slow spontaneous nucleotide cycling [11], in vivo, their activity is tightly controlled by a number of regulatory molecules. Guanine nucleotide exchange factors (GEFs) activate the GTPases by catalyzing the replacement of bound GDP by GTP. Conversely, GTPase activating proteins (GAPs) deactivate the GTPases by facilitating the hydrolysis of GTP into GDP. In addition, GDP dissociation inhibitors (GDIs) reversibly associate with the inactive form of the Rho GTPases and participate in their membrane-cytoplasmic shuttling and intracellular transport [1].

Formation of the incipient yeast bud can be naturally subdivided into two consecutive phases [12,13]. During the short initial phase, a round cluster of activated Cdc42 forms on the inner leaflet of the plasma membrane in a location predetermined by the landmark proteins, which in haploid yeast are positioned around the bud scar remaining from the previous cell division [10]. Subsequent recruitment of the Cdc42 effectors results in the formation of actin cables and a concentric septin ring that defines the bud neck. In the ensuing phase of growth and protrusion, the actin cables serve as tracks for polarized exocytosis of vesicles that bring material for the bud growth. Importantly, it has been shown that neither actin nor landmark proteins are essential for the emergence of the Cdc42 cluster [12,14]. Instead, this phase requires the Cdc42 GEF Cdc24, the Cdc42 effector Bem1 and the ability of the GTPase to cycle between the active GTP-bound and inactive GDP-bound states [13,14]. In sharp contrast, the following actin-dependent phase has been shown to successfully proceed with a constitutively active version of Cdc42 which did not require Cdc24 or Bem1 [13,15]. In natural conditions, transport vesicles are thought to deliver inactive Cdc42 [15] whose local activation is required for polarized exocytosis at the incipient yeast bud [16]. Apart from this common requirement for Cdc42 and its regulatory molecules, the

*Corresponding author.
E-mail address: Andrew.Goryachev@ed.ac.uk (A.B. Goryachev).

Abbreviations: GEF, guanine nucleotide exchange factor; GAP, GTPase activating protein

0014-5793/$34.00
doi:10.1016/j.febslet.2008.03.029

two phases of bud formation rely on distinct molecular mechanisms. Here we focus on the formation of the Cdc42 cluster as the primary symmetry-breaking event that provides a prepattern for the subsequent morphogenesis. We assumed that the non-essential landmark proteins had been deleted [13,14] to exclude any preexisting spatial cues and that the transition to the succeeding actin-dependent phase had been arrested by treatment with latranculin A, a standard actin-depolymerizing agent. The growth and protrusion phase which is dependent on the actin-directed exocytosis has been studied in detail elsewhere [15,17] and is not considered further in this report.

2. Materials and methods

To understand emergence of the cluster of activated Cdc42 during the early phase of yeast bud formation, we developed a whole-cell model that describes reactions, membrane-cytoplasmic shuttling and diffusion of the essential molecules. It was assumed that, on the time scale of the cluster formation, production and degradation of proteins can be neglected. Therefore the total intracellular amounts of Cdc42, its GEF Cdc24 and effector Bem1 were kept constant. The resulting system of reaction–diffusion equations was simulated numerically and analyzed using several complementary methods. A detailed description of methods including the derivation of model equations, parameter selection, model analysis and its computational implementation are provided in the Supplementary Methods.

3. Results and discussion

Analysis of a large body of experimental data brought us to the conclusion that Cdc42 nucleotide cycling and membrane-cytoplasmic shuttling are the two processes responsible for the formation of the Cdc42 cluster on the membrane [13,14]. Cytoplasmic Cdc42 is the inactive GDP-bound form (RD) found in a complex with RhoGDI proteins that reversibly deposit the RD on the membrane and recycle it back to the cytoplasm [1,18] (Fig. 1E and Supplementary Methods). Cdc24 and Bem1 also shuttle between the membrane and the cytoplasm on their own or as a heterodimer. Importantly, formation of the Cdc24 · Bem1 complex increases the retention of Cdc24 on the membrane in the catalytically potent form that can activate the membrane-bound RD [14,19]. Active Cdc42 (RT) is thought to remain on the membrane until deactivated by a GAP [1] and in turn binds and activates its various effectors, including Bem1 [10,14]. The binding of Bem1 to RT recruits the Cdc24 · Bem1 complex from the cytoplasm and further increases the retention of Cdc24 through the formation of a trimolecular complex [19,20]. Once activated and stabilized on the membrane by RT and Bem1, Cdc24 in a positive feedback loop generates more membrane-bound RT at the expense of the Cdc42 cytoplasmic store [13,14,21].

3.1. Cluster of activated Cdc42 forms spontaneously in the model of bud formation

To understand the forces that drive the emergence of the Cdc42 cluster, we constructed and analyzed a detailed mathematical model of the cluster formation. Chemical reactions, membrane-cytoplasmic exchange and diffusion of all essential species were represented as a system of partial differential equations which was solved numerically (see Supplementary Methods).

In vivo, the formation of a new bud in haploid wild-type yeast is initiated by the cell-cycle regulated release of Cdc24 from the cell nucleus [22]. In silico, starting with the spatially homogeneous distribution of Cdc42 and Cdc24 · Bem1 complex in the cytoplasm and no RT on the membrane, the model evolved into a steady-state with RT uniformly distributed over the membrane. On closer investigation, this stationary state was found to be unstable to spatially heterogeneous perturbations. Astonishingly, the perturbed uniform state evolved into a striking asymmetric pattern with all RT assembled in a single round cluster with a bell-shaped concentration profile as shown in Fig. 1A. Exactly the same structure emerged when we started simulations with RT non-uniformly seeded on the membrane. Insensitive to the initial conditions, the Cdc42 cluster was found dependent on variation of the diffusion coefficients. Gradual reduction of the cytoplasmic diffusivity D_c, or increase in the membrane diffusivity D_m, resulted in spreading and eventual dissolution of the structure into a stable uniform state.

3.2. Stationary cytoplasmic flux offsets diffusive spread of the cluster

As the cluster persisted indefinitely in our simulations, we asked which mechanism counteracts the diffusion that tends to uniformly distribute RT over the membrane. We found that in the stationary state the inevitable diffusive spread of the cluster on the membrane is exactly compensated by a cytoplasmic flux of the cluster components as shown in Fig. 1. Importantly, since the active form of Cdc42 is essentially membrane-bound, the GDI-mediated membrane-cytoplasmic traffic of the GTPase is entirely determined by the balance of the cytoplasmic and membrane pools of the inactive form. Far away from the cluster, association of RD with the membrane is exactly balanced by its dissociation resulting in a steady-state membrane concentration RD_0 and a zero membrane-cytoplasmic flux $J_0 = 0$ (Fig. 1 C and D). However, in the center of the cluster, rapid activation of Cdc42 (RD → RT) by the highly concentrated GEF complex causes local depletion of RD, $RD_C < RD_0$, and thus favors the deposition of Cdc42 over its return to the cytoplasm, $J_C > 0$. As RT diffuses along the membrane away from the cluster center, the concentration of the GEF complex sharply drops and the inactivation of Cdc42 by the GAPs becomes the predominant reaction (RT → RD) (Fig. 1E). This causes local excess of RD at the cluster periphery, $RD_P > RD_0$, and, consequently, GDI-mediated dissociation of Cdc42 from the membrane, $J_P < 0$. The coupling of the Cdc42 membrane-cytoplasmic shuttling and its nucleotide cycling results in the net deposition of Cdc42 in the cluster center and the return back to the cytoplasm at the cluster periphery (Fig. 1E). GEF complex Cdc24 · Bem1 shuttles between the membrane and the cytoplasm together with Cdc42 and the steady-state profile of the Cdc24 · Bem1 flux (Fig. 1D, green) is qualitatively identical to that of Cdc42. To maintain this cyclic flux of Cdc42 in the steady-state requires a continuous supply of energy which is provided by the hydrolysis of GTP during the Cdc42 nucleotide cycling. The resulting spatial profile of the membrane-cytoplasmic transport shown in Fig. 1D is characteristic of local activation and lateral inhibition, the two fundamental properties that were found essential for the formation of spatial patterns in a variety of biological systems [3,23].

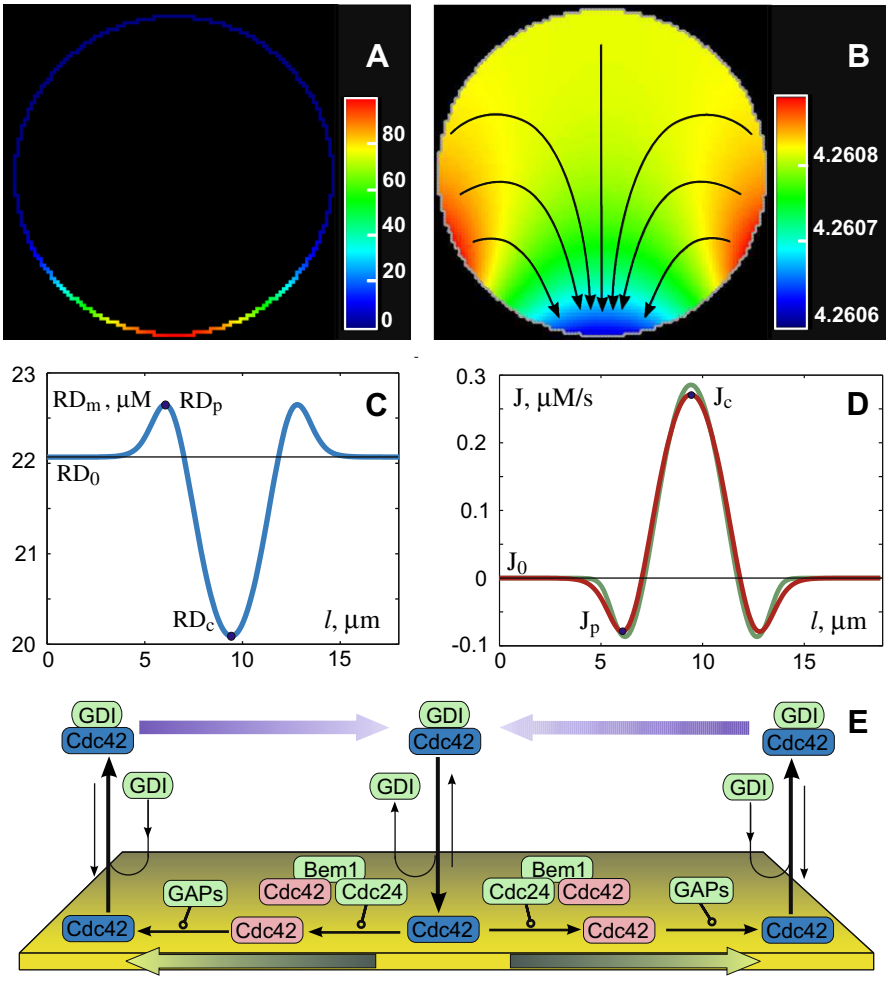

Fig. 1. Self-organized cluster of activated Cdc42 is maintained in the steady-state by a continuous membrane-cytoplasmic flux. (A and B) 2D cross-section of a yeast cell simulated with Virtual Cell [36]. (A) Distribution of the activated Cdc42 on the membrane (RT, μM) qualitatively reproduces experimental results [14,17]. (B) Concentration of the inactive Cdc42 · GDI complex in the cytoplasm (RDIc, μM). Stationary cytoplasmic flux of RDIc (arrows) compensates diffusive spread of the cluster on the membrane. (C) Steady-state profile of the inactive Cdc42 (RD) on the membrane plotted along the cellular circumference shows depletion in the cluster center and excess on its periphery. (D) Membrane-cytoplasmic fluxes of Cdc42 (red) and Cdc24 · Bem1 complex (green). Positive value indicates net flux direction towards the membrane. For visual clarity, the Cdc24 · Bem1 flux is multiplied by 10. (E) Cartoon explaining how the membrane-cytoplasmic shuttling of Cdc42 (inactive form, blue; active, pink) is coupled to its nucleotide cycling in the cluster. Thick black arrows represent the predominant direction of the membrane-cytoplasmic exchange; open circle arrowheads indicate catalysis; colored arrows represent the diffusion flux direction on the membrane and in the cytoplasm.

3.3. Cdc42 cluster is robust to parameter variation and molecular noise

Robustness to fluctuations in the reaction rates and species concentrations has been proposed as a major property of naturally evolved molecular networks. We thus set out to explore how variation of the model parameters affects the concentration profile of the Cdc42 cluster. Varying the reaction rates and computing the change in the maximum concentration and the width of the stationary RT profile, we found that the cluster is indeed largely insensitive to these variations (see Table S2 in Supplementary Methods).

More importantly, our model robustly reproduced the formation of a unique Cdc42 cluster in the experiments with deleted landmark proteins and a depolymerized actin cytoskeleton [13,14]. In the absence of spatial cues provided by the landmarks, the yeast bud is known to form at a random, yet unique, location. We simulated the emergence of the Cdc42 cluster under the conditions of molecular noise by taking into the consideration spontaneous activation of individual Cdc42 molecules on the membrane (see Supplementary Methods). This noise was sufficient to initiate the accumulation of RT on the membrane, at first without clear spatial preference (Fig. 2). However, as the accumulation continued, readily distinguishable cluster nuclei formed and competed with each other. We performed a large number of simulations varying the specific realization of the random molecular noise as well as its intensity. In all simulations, only one of the nuclei developed into a mature stationary cluster in accord with the experimental observations (see also Movie S1). This demonstrated that molecular noise is sufficient to induce spontaneous Cdc42 cluster formation. Despite random induction of multiple nucleation cores, only one mature cluster emerged from the competition of the nuclei regardless of the particular noise realization.

The standard linear stability analysis of the uniform stationary state of the model confirmed our numeric simulations and

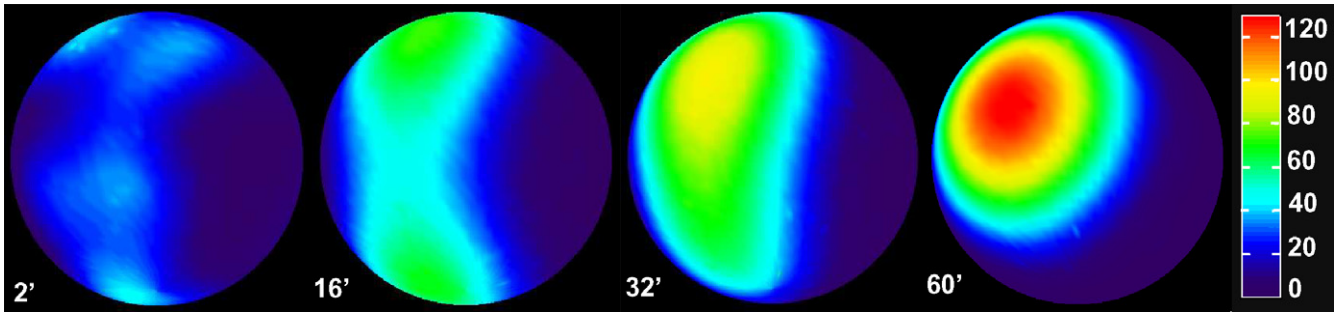

Fig. 2. A single Cdc42 cluster forms in the simulations with molecular noise. A 3D view on the surface of a yeast cell shows the distribution of the activated Cdc42 on the membrane, coded by color (RT, μM). In the absence of landmark proteins, spontaneous activation of individual Cdc42 molecules on the membrane can induce the cluster formation. Initially, all Cdc24 · Bem1 is in the cytoplasm. At first, RT accumulates at multiple random locations (2 min). Subsequently, two well-defined cluster nuclei form (16 min). The top nucleus consumes the slower-growing lower nucleus (32 min). By 1 h the Cdc42 cluster is near the steady-state.

proved that the spontaneous formation of the Cdc42 cluster observed in our in silico experiments is indeed a genuine diffusion-driven instability (Fig. S1 in Supplementary Methods). Furthermore, this analysis suggested that the structure that emerges out of the unstable uniform state could be a mixture of three distinct patterns: a single cluster, two opposing clusters and three equidistant clusters. In simulations, however, we found that patterns with multiple identical clusters are also unstable to perturbations and, once destabilized, invariably evolve into a single cluster that amasses all of the material of the initial clusters. Thus, we explain the uniqueness of the Cdc42 cluster by the competition of the candidate clusters for shared resources, the cellular stores of Cdc42, Cdc24 and especially Bem1, which is the least abundant cluster component in the yeast cell [24].

3.4. Network motif responsible for the Cdc42 cluster formation

Next, we asked which elements of the reaction network are directly responsible for the destabilization of the uniform RT distribution and the emergence of the cluster. Using the techniques of graph-theoretic analysis [25] (see Supplementary Methods), we traced the cause of the Turing-type instability in our model to the network cycle shown in Fig. 3. The cycle represents a positive feedback loop in which the membrane-bound RT recruits Cdc24 · Bem1 from the cytoplasm and forms a highly active Cdc24 · Bem1 · RT complex that generates more RT from RD [26]. In silico, we disabled the interaction between RT and the cytoplasmic Cdc24 · Bem1 (reaction v_8 in Fig. 3B). In complete agreement with the graph analysis, the disruption of this autocatalytic loop totally abrogated the formation of the Cdc42 cluster. Importantly, another autocatalytic loop, which is structurally identical to the cycle in Fig. 3 but instead involves the membrane-bound Cdc24 · Bem1 complex, cannot rescue the cluster formation (see Supplementary Methods). This striking result may be explained by the necessity to maintain the membrane-cytoplasmic circulation of the cluster components. Indeed, the interaction between the cytoplasmic Cdc24 · Bem1 and membrane-bound RT couples the spatio-temporal dynamics of Cdc24 to the GTP-driven membrane-cytoplasmic flux of Cdc42. The loss of this interaction does not prevent the autocatalytic production of RT but rather terminates the recruitment of Cdc24 from the cytoplasm into the cluster.

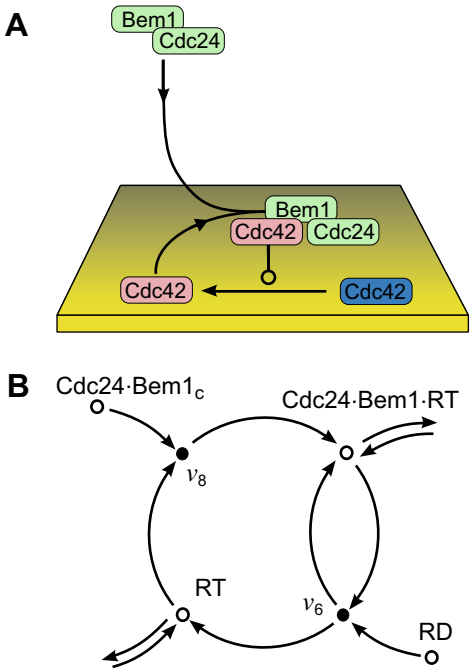

Fig. 3. Positive feedback loop with autocatalytic production of activated Cdc42 destabilizes the spatially uniform steady-state and causes the formation of the Cdc42 cluster. (A) Loop diagram, notations are the same as in Fig. 1. (B) The corresponding bi-partite reaction graph (see Supplementary Methods). Species and reactions are represented by open and filled circles, respectively. The complete reaction network graph is shown in Fig. S2.

Our results demonstrate that this process is essential for the growth and maintenance of the cluster.

3.5. Turing-type model emerges from the complete reaction–diffusion mechanism

Reduction of large models to their minimal functional form has been proven beneficial for uncovering fundamental features often buried in complex reaction mechanisms. Assuming a number of simplifying approximations (see Supplementary Methods), we reduced our complete model to a model with only two variables: RT (X) and the total concentration of the inactive Cdc42 (Y):

$$\dot{x} = E_c\alpha x^2 y + E_c\beta xy - \gamma x + D_m\Delta x,$$
$$\dot{y} = \gamma x - E_c\alpha x^2 y - E_c\beta xy + D_c\Delta y,$$
$$E_c = E_c^0\left(1 + \int_S f(x)\mathrm{d}s\right)^{-1}.$$

The last equation represents conservation of the total cellular amount of Cdc24 · Bem1. Depletion of Cdc24 · Bem1 prevents the recruitment of the entire cytoplasmic Cdc42 into the cluster and thus has to be captured by the model. The reduced model belongs to the prototypical activator–substrate type [23] in which the slowly diffusing activator X autocatalytically reproduces itself at the expense of the fast diffusing substrate Y. In our reduced model, the autocatalytic production of X occurs through the parallel cubic $2X + Y \to 3X$ and quadratic $X + Y \to 2X$ effective mechanisms that correspond to two different pathways of RT generation. The effectively cubic mechanism emerges from the reduction of the critical fragment of the complete reaction network (Fig. 3). The respective term of the reduced model, $E_c\alpha x^2 y$, essentially represents the product of three reactions: (i) recruitment of the cytoplasmic Cdc24 · Bem1 to the membrane (reaction rate proportional to the concentration of the recruiting RT, i.e., x); (ii) formation of the activated GEF complex Cdc24 · Bem1 · RT (brings in another factor x); (iii) activation of RD by the Cdc24 · Bem1 · RT complex (proportional to y). The other mechanism corresponds to the pathway that does not include the recruitment of the cytoplasmic Cdc24 · Bem1 and comprises only the reactions (ii) and (iii). The respective term, $E_c\beta xy$, is thus quadratic.

Importantly, only the cubic mechanism supports the formation of the Cdc42 cluster. The quadratic term alone was not sufficient to produce the cluster in the reduced model. This is in the complete agreement with our graph-theoretic analysis since the loss of the cubic mechanism in the reduced model is equivalent to disruption of the critical fragment shown in Fig. 3. Interestingly, cubic autocatalysis is typical for the two-variable models of pattern formation that were developed in various disciplines [27] (see Fig. 4). The apparent similarity of the reaction graphs of our model and the Brusselator highlights their common principle of pattern formation. In both models the deactivation pathway $X \to Y$ dominates at low concentrations of X. Only above a certain threshold concentration X^* does the autocatalytic production of X prevails over its deactivation and the net direction of the reaction flux reverses $Y \to X$.

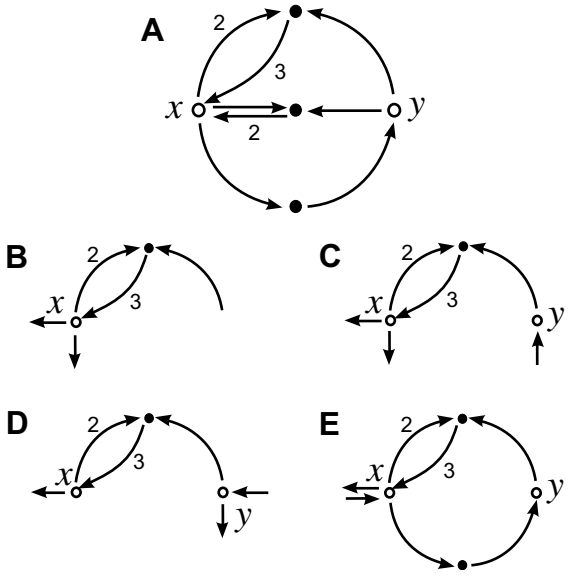

Fig. 4. The reduced model of the Cdc42 cluster formation belongs to a well-known class of activator–substrate models with autocatalysis [3]. Graph representation reveals common and divergent features of the reaction mechanisms typical of this class: (A) Reduced Cdc42 cluster formation model; (B) one-variable Schlögl model; (C) Schnakenberg model; (D) Gray-Scott model; (E) Brusselator. Species and reactions are denoted as open and filled circles, respectively. The stoichiometric coefficients on the arrows correspond to the cubic $2X + Y \to 3X$ and quadratic $X + Y \to 2X$ autocatalytic mechanisms.

4. Conclusions

Turing-type models have long been anticipated to describe the self-organized emergence of cellular polarity, however, the underlying molecular networks were largely unknown. In this study we started with the detailed, experimentally determined molecular mechanism based on the small Rho GTPase Cdc42 [26]. Using complementary methods of biophysical modeling, mathematical biology and graph-theoretic analysis we demonstrated that the molecular network consisting of Cdc42, its regulatory molecules and an effector can explain the spontaneous emergence of cellular polarization in yeast through the Turing-type instability. This phenomenon is robust to variation of reaction rates and molecular noise. Importantly, our results demonstrate that the roles of both the activator and substrate in the prototypical Turing mechanism can be played by a single molecular species with two distinct states. We hypothesize that small GTPases have evolved to perform this double function in a variety of cellular processes that require rapid formation of compact protein clusters on the membranes. This hypothesis is based on the observation that the network motif demonstrated here to be essential for the formation of the cluster is found experimentally in the rapidly increasing number of biological systems [26,28]. Indeed, GTPase effectors that recruit and activate a GEF for the same GTPase have been identified in the molecular networks that control exocytosis [29], fusion

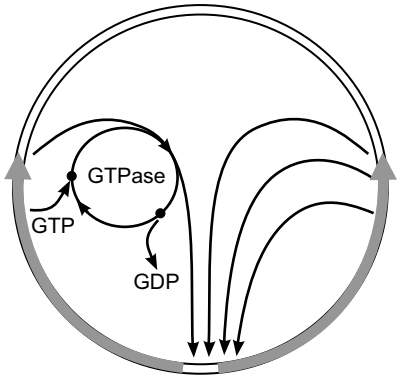

Fig. 5. Schematic representation of the mechanism underlying stable existence of the cluster of activated Cdc42 on the yeast cell membrane. Driven by the continuous expenditure of cellular energy (GTP), stationary membrane-cytoplasmic flux of cluster components (thin arrows) compensates for the inevitable diffusive spread of the cluster on the membrane (thick arrows).

of early endosomes [30] and yeast vacuoles [31]. A peculiar example of this network motif, implemented as a single protein with complex regulation, is represented by Sos (son of sevenless), the protein that possesses both the effector and GEF domains for Ras GTPase [32].

The cluster of activated Cdc42 that marks the presumptive bud site is shown here to be a true dissipative structure as defined by Ilya Prigogine [33] since its emergence and maintenance require continuous expenditure of the cellular energy stored as GTP (see Fig. 5). This explains the experimentally found requirement for the Cdc42 nucleotide cycling during which GTP is hydrolyzed. Corroborating the ideas proposed in [34], we conclude that small GTPases utilize cellular energy to combat the inevitable increase in entropy, manifested by the diffusive spread of the Cdc42 cluster on the membrane. The robust uniqueness of the yeast bud is explained in our model by the resource competition that destabilizes the coexistence of multiple buds. For a few known yeast mutants that can grow several buds simultaneously, the cause of the abnormality was traced to the altered control of nucleotide cycling [35]. It would be interesting to extend our model to incorporate these mutants and characterize the nature of multiple budding.

Acknowledgements: We thank M. Mincheva, M.R. Roussel and G. Ermakov for help with the graph-theoretic analysis of reaction networks; D.J. Lew, A.J. Millar, N.D. Read, K.E. Sawin and K.J. Painter for many stimulating discussions and helpful suggestions. A.B.G. is supported by the RCUK Academic Fellowship.

Appendix A. Supplementary data

Supplementary data associated with this article can be found, in the online version, at doi:10.1016/j.febslet.2008.03.029.

References

[1] Jaffe, A.B. and Hall, A. (2005) Rho GTPases: biochemistry and biology. Annu. Rev. Cell Dev. Biol. 21, 247–269.
[2] Fukata, M., Nakagawa, M. and Kaibuchi, K. (2003) Roles of Rho-family GTPases in cell polarisation and directional migration. Curr. Opin. Cell Biol. 15, 590–597.
[3] Maini, P.K., Painter, K.J. and Chau, H.N.P. (1997) Spatial pattern formation in chemical and biological systems. J. Chem. Soc. Faraday Trans. 93, 3601–3610.
[4] Turing, A.M. (1952) The chemical basis of morphogenesis. Philos. Trans. R. Soc. Lond. B: Biol. Sci. 237, 37–72.
[5] Meinhardt, H. (1999) Orientation of chemotactic cells and growth cones: models and mechanisms. J. Cell Sci. 112, 2867–2874.
[6] Levchenko, A. and Iglesias, P.A. (2002) Models of eukaryotic gradient sensing: application to chemotaxis of amoebae and neutrophils. Biophys. J. 82, 50–63.
[7] Narang, A. (2006) Spontaneous polarization in eukaryotic gradient sensing: a mathematical model based on mutual inhibition of frontness and backness pathways. J. Theor. Biol. 240, 538–553.
[8] Maly, I.V., Wiley, H.S. and Lauffenburger, D.A. (2004) Self-organization of polarized cell signaling via autocrine circuits: computational model analysis. Biophys. J. 86, 10–22.
[9] Maini, P.K., Baker, R.E. and Chuong, C.M. (2006) Developmental biology. The Turing model comes of molecular age. Science 314, 1397–1398.
[10] Park, H.O. and Bi, E. (2007) Central roles of small GTPases in the development of cell polarity in yeast and beyond. Microbiol. Mol. Biol. Rev. 71, 48–96.
[11] Zhang, B., Zhang, Y., Wang, Z. and Zheng, Y. (2000) The role of Mg^{2+} cofactor in the guanine nucleotide exchange and GTP hydrolysis reactions of Rho family GTP-binding proteins. J. Biol. Chem. 275, 25299–25307.
[12] Ayscough, K.R., Stryker, J., Pokala, N., Sanders, M., Crews, P. and Drubin, D.G. (1997) High rates of actin filament turnover in budding yeast and roles for actin in establishment and maintenance of cell polarity revealed using the actin inhibitor latrunculin-A. J. Cell Biol. 137, 399–416.
[13] Wedlich-Soldner, R., Wai, S.C., Schmidt, T. and Li, R. (2004) Robust cell polarity is a dynamic state established by coupling transport and GTPase signaling. J. Cell Biol. 166, 889–900.
[14] Irazoqui, J.E., Gladfelter, A.S. and Lew, D.J. (2003) Scaffold-mediated symmetry breaking by Cdc42p. Nat. Cell Biol. 5, 1062–1070.
[15] Wedlich-Soldner, R., Altschuler, S., Wu, L. and Li, R. (2003) Spontaneous cell polarization through actomyosin-based delivery of the Cdc42 GTPase. Science 299, 1231–1235.
[16] Zhang, X., Bi, E., Novick, P., Du, L., Kozminski, K.G., Lipschutz, J.H. and Guo, W. (2001) Cdc42 interacts with the exocyst and regulates polarized secretion. J. Biol. Chem. 276, 46745–46750.
[17] Marco, E., Wedlich-Soldner, R., Li, R., Altschuler, S.J. and Wu, L.F. (2007) Endocytosis optimizes the dynamic localization of membrane proteins that regulate cortical polarity. Cell 129, 411–422.
[18] Dovas, A. and Couchman, J.R. (2005) RhoGDI: multiple functions in the regulation of Rho family GTPase activities. Biochem. J. 390, 1–9.
[19] Shimada, Y., Wiget, P., Gulli, M.P., Bi, E. and Peter, M. (2004) The nucleotide exchange factor Cdc24p may be regulated by auto-inhibition. EMBO J. 23, 1051–1062.
[20] Bose, I., Irazoqui, J.E., Moskow, J.J., Bardes, E.S., Zyla, T.R. and Lew, D.J. (2001) Assembly of scaffold-mediated complexes containing Cdc42p, the exchange factor Cdc24p, and the effector Cla4p required for cell cycle-regulated phosphorylation of Cdc24p. J. Biol. Chem. 276, 7176–7186.
[21] Butty, A.C., Perrinjaquet, N., Petit, A., Jaquenoud, M., Segall, J.E., Hofmann, K., Zwahlen, C. and Peter, M. (2002) A positive feedback loop stabilizes the guanine-nucleotide exchange factor Cdc24 at sites of polarization. EMBO J. 21, 1565–1576.
[22] Gulli, M.P., Jaquenoud, M., Shimada, Y., Niederhauser, G., Wiget, P. and Peter, M. (2000) Phosphorylation of the Cdc42 exchange factor Cdc24 by the PAK-like kinase Cla4 may regulate polarized growth in yeast. Mol. Cell 6, 1155–1167.
[23] Murray, J.D. (1993) Mathematical Biology, Springer-Verlag, Berlin.
[24] Ghaemmaghami, S., Huh, W.K., Bower, K., Howson, R.W., Belle, A., Dephoure, N., O'Shea, E.K. and Weissman, J.S. (2003) Global analysis of protein expression in yeast. Nature 425, 737–741.
[25] Mincheva, M. and Roussel, M.R. (2006) A graph-theoretic method for detecting potential Turing bifurcations. J. Chem. Phys. 125, 204102.
[26] Goryachev, A.B. and Pokhilko, A.V. (2006) Computational model explains high activity and rapid cycling of Rho GTPases within protein complexes. PLoS Comput. Biol. 2, e172.
[27] Tyson, J.J. and Light, J.C. (1973) Properties of two-component bimolecular and trimolecular chemical reaction systems. J. Chem. Phys. 59, 4164–4172.
[28] Grosshans, B.L., Ortiz, D. and Novick, P. (2006) Rabs and their effectors: achieving specificity in membrane traffic. Proc. Natl. Acad. Sci. USA 103, 11821–11827.
[29] Medkova, M., France, Y.E., Coleman, J. and Novick, P. (2006) The rab exchange factor Sec2p reversibly associates with the exocyst. Mol. Biol. Cell 17, 2757–2769.
[30] Lippe, R., Miaczynska, M., Rybin, V., Runge, A. and Zerial, M. (2001) Functional synergy between Rab5 effector Rabaptin-5 and exchange factor Rabex-5 when physically associated in a complex. Mol. Biol. Cell 12, 2219–2228.
[31] Wurmser, A.E., Sato, T.K. and Emr, S.D. (2000) New component of the vacuolar class C-Vps complex couples nucleotide exchange on the Ypt7 GTPase to SNARE-dependent docking and fusion. J. Cell Biol. 151, 551–562.
[32] Margarit, S.M., Sondermann, H., Hall, B.E., Nagar, B., Hoelz, A., Pirruccello, M., Bar-Sagi, D. and Kuriyan, J. (2003) Structural

evidence for feedback activation by Ras · GTP of the Ras-specific nucleotide exchange factor SOS. Cell 112, 685–695.
[33] Glansdorff, P. and Prigogine, I. (1971) Thermodynamic Theory of Structure, Stability and Fluctuations, John Wiley, New York.
[34] Goody, R.S. (2003) The significance of the free energy of hydrolysis of GTP for signal-transducing and regulatory GTPases. Biophys. Chem. 100, 535–544.
[35] Caviston, J.P., Tcheperegine, S.E. and Bi, E. (2002) Singularity in budding: a role for the evolutionarily conserved small GTPase Cdc42p. Proc. Natl. Acad. Sci. USA 99, 12185–12190.
[36] Schaff, J., Fink, C.C., Slepchenko, B., Carson, J.H. and Loew, L.M. (1997) A general computational framework for modeling cellular structure and function. Biophys. J. 73, 1135–1146.

Supplementary Methods

Detailed reaction mechanism and the model formulation

Rho GTPase Cdc42, its GEF Cdc24 and effector Bem1 are the three molecular species whose interactions are essential for the formation of the cluster of activated Cdc42 [1,2]. The majority of cellular Cdc42 is thought [3] to exist as a complex, RDI, of the inactive GDP-bound form RD and a RhoGDI protein denoted here as I. RDI binds to the membrane although the majority of RDI remains cytoplasmic. Binding to the membrane, however, facilitates dissociation of the RDI into the membrane-bound RD and the cytoplasmic I [4,5]. The dynamic equilibrium of the two reversible reactions, the binding of RDI to the membrane and RDI dissociation, results in the continuous shuttling of RD between the membrane and the cytoplasm.

Nucleotide cycling of Cdc42 is catalyzed by the GEF Cdc24 and the three GAPs Bem3, Rga1 and Rga2 [6]. Since the individual contributions of the GAPs are not yet clearly defined, we assumed a single effective GAP species A that is homogeneously distributed in the cytoplasm with the concentration A_0. Cdc24 and Bem1 are known to form a stable complex through the binding of their PB1 domains [7,8]. The destabilization of this complex requires phosphorylation of Cdc24 by the Cdc42 effector Cla4, the event that occurs after the formation of the Cdc42 cluster, well within the subsequent actin-dependent phase of the yeast bud formation [9]. We, therefore, assumed that Bem1 and Cdc24 remain in a complex E throughout the formation of the Cdc42 cluster and the dissociation of E can be neglected. To test the validity of this simplification, we increased the complexity of the model by considering Cdc24, Bem1 and their complex E as three independent species. Numerical simulation of this higher-dimensional model however demonstrated no qualitative differences with our main model. E weakly associates with the membrane and thus also shuttles between the membrane and the cytoplasm. While on the membrane, it can bind RD and convert it into the active RT. Through the effector domain of Bem1, E reversibly associates with RT forming a trimolecular complex M. Following [10], we hypothesized that M has a more potent GEF activity towards RD than E. This hypothesis is based on a steadily increasing number of reports that describe tripartite complexes consisting of an activated small GTPase, its effector and a GEF for the same GTPase [11]. Several lines of evidence, including quantitative biochemical characterization [12], indicate that binding of the activated GTPase to the effector increases the activity of the effector-bound GEF by several fold [13], thus generating a positive feedback loop.

Using mass-action rate laws for the described above mechanism, we developed a whole-cell model with spatially-distributed cytoplasmic and membranous compartments. Our model consists of eight reaction-diffusion equations:

$$
\begin{aligned}
\frac{\partial RT}{\partial t} &= (k_2 E_m + k_3 M)\cdot RD - k_{-2} RT - k_4 E_m \cdot RT + k_{-4} M - k_7 E_c \cdot RT + D_m \Delta RT \\
\frac{\partial M}{\partial t} &= k_4 E_m \cdot RT - k_{-4} M + k_7 E_c \cdot RT + D_m \Delta M \\
\frac{\partial E_m}{\partial t} &= k_1 E_c - k_{-1} E_m - k_4 E_m \cdot RT + k_{-4} M + D_m \Delta E_m \\
\frac{\partial E_c}{\partial t} &= \eta\left[k_{-1} E_m - (k_1 + k_7 RT) E_c\right] + D_c \Delta E_c \\
\frac{\partial RD}{\partial t} &= k_{-2} RT - (k_2 E_m + k_3 M)\cdot RD + k_{-6} RDI_m - k_6 I \cdot RD + D_m \Delta RD \\
\frac{\partial RDI_m}{\partial t} &= k_6 I \cdot RD - k_{-6} RDI_m + k_5 RDI_c - k_{-5} RDI_m + D_m \Delta RDI_m \\
\frac{\partial RDI_c}{\partial t} &= \eta\left[k_{-5} RDI_m - k_5 RDI_c\right] + D_c \Delta RDI_c \\
\frac{\partial I}{\partial t} &= \eta\left[k_{-6} RDI_m - k_6 I \cdot RD\right] + D_c \Delta I
\end{aligned}
\qquad (1)
$$

Species RT, RD and M are strictly membrane-bound, I is cytoplasmic, while RDI and E exist both on the membrane and in the cytoplasm as indicated by the respective subscripts. Following the approach developed in [14,15], the concentrations of cytoplasmic species were computed per cytoplasmic volume V_c, while concentrations of the membrane-bound species per smaller volume V_m, which represents a thin ($\approx 10\ nm$) layer of cytoplasm immediately adjacent to the membrane. To account for this difference, scaling coefficient $\eta = V_m / V_c$ was introduced in the equations for the cytoplasmic species. Assuming yeast cell to be a sphere with the diameter $6\mu m$, we estimated the scaling coefficient as $\eta = 0.01$.

For simplicity, all cytoplasmic and membrane-bound species were assumed to diffuse with a single compartment-specific diffusion coefficient D_c and D_m, respectively. D_c was varied in the range $1 \div 10\,\mu m^2/s$, which is typical for the small to medium-sized proteins in the cytoplasm [16]. Based on several accounts of anomalously slow diffusion on the yeast membrane [17,18], we adopted the value of membrane diffusivity $D_m = 0.0025\,\mu m^2/s$.

The deactivation of RT into RD through the spontaneous and GAP-catalyzed channels is represented in our model as a single, effectively first order reaction with the composite reaction rate constant $k_{-2} = k_{-2,0} + k_{-2,1} \cdot A_0$. The values of all rate constants together with their sources are listed in the Table S1.

Computational implementation

Several computational strategies have been used to simulate the model *in silico*. In all approaches the yeast cell was approximated by a sphere with diameter of $6\mu m$. Axial symmetry of the budding cell was utilized to reduce computational cost by simulating the complete reaction-diffusion model on the cellular cross-section. These simulations were performed using the premier computational cell biology platform Virtual Cell [19]. Varying cytoplasmic diffusion coefficient in these simulations, we observed that the increase of the cytoplasmic diffusion coefficient D_c beyond its estimated value of $10\,\mu m^2/s$ does not noticeably change the concentration profile of the Cdc42 cluster (see also Figure S1). Indeed, at large D_c the cytoplasmic fluxes of Cdc42 and its GEF Cdc24 that define the stationary shape of the cluster are limited by the traffic at the membrane-cytoplasm interface and not by the diffusion of molecules through the cytoplasm. Taking advantage of this fact, we simulated the formation of the Cdc42 cluster on the entire cell membrane in the limit of infinite cytoplasmic diffusivity $D_c \to \infty$, thus, neglecting spatial variation in the concentrations of cytoplasmic species. Under this assumption the simulation of our model could be again reduced to an effectively two-dimensional computational problem. The calculations were performed on a spherical surface using the finite difference algorithm [20] implemented as a C code. Varying mesh sizes, algorithms and switching from the sphere to torus, we verified that the computed properties of the Cdc42 cluster are not affected by the choice of a computational method or the topology of the mesh.

To simulate molecular noise necessary to induce the cluster formation in the absence of landmark proteins, we first evaluated the average number of the RT molecules produced on the cell surface due to the spontaneous activation $RD \to RT$. Using our detailed kinetic model of the GTPase cycle [10], we obtained an estimate for the average noise intensity of 6 molecules per second per cell. To simulate random activation events, we then generated random process with Poisson distribution in time and uniform distribution in space. Variation of the noise intensity did not result in qualitative differences in the model behavior.

All algorithms and codes used in this work are freely available on request from the authors.

Parametric robustness of the Cdc42 cluster

Using the stationary Cdc42 cluster at the parameter values given in the Table S1 as the reference state, we computed parametric sensitivity of the cluster RT concentration profile as follows. Each parameter was separately increased by the factor of 2 and the model was allowed to reach the new stationary state. We chose the maximal concentration of RT in the cluster and the cluster width as the response variables. They

were computed for each perturbed parameter and normalized by the respective reference values to produce relative deviations reported in the Table S2. To avoid ambiguity in the definition of the cluster width, it was computed as the distance between the points where the stationary membrane-cytoplasmic flux of RD changed its sign (see Figure 1D). The same procedure was repeated with each parameter reduced by the factor of 2.

Stoichiometric analysis of the model

To simplify the analysis of the reaction mechanism, it is convenient to eliminate the explicit dependence of model (1) on the scaling coefficient η. This can be readily achieved by rescaling the three cytoplasmic variables, e.g., $E_c^* = E_c/\eta$, and the four rate constants, k_1, k_5, k_6, k_7, which describe the association of the cytoplasmic molecules with the membrane, e.g., $k_1^* = \eta k_1$. Unless specified otherwise, this scaling is assumed in the following analysis and the star superscripts are dropped for simplicity.
To represent the reaction mechanism in the formal terms of the stoichiometric network analysis (SNA) [21], we introduced the model reaction rates as follows:

$$\begin{aligned} &v_1 = k_1 E_c,\ v_2 = k_{-1} E_m,\ v_3 = k_4 E_m \cdot RT,\ v_4 = k_{-4} M, \\ &v_5 = k_2 E_m \cdot RD,\ v_6 = k_3 M \cdot RD,\ v_7 = k_{-2} RT,\ v_8 = k_7 E_c \cdot RT, \\ &v_9 = k_{-6} RD\,\mathrm{I_m},\ v_{10} = k_6 I_c \cdot RD,\ v_{11} = k_5 RDI_c,\ v_{12} = k_{-5} RD\,\mathrm{I_m} \end{aligned} \tag{2}$$

Using these notations, the reaction part of model (1) can be represented simply as

$$\frac{d\mathbf{s}}{dt} = \mathbf{N} \bullet \mathbf{v}, \tag{3}$$

where **s** is the vector of species concentrations, which are numbered according to their sequence in (1), i.e., $s_1 = RT,\ s_2 = M,$ etc., **v** is the vector of reaction rates as defined in (2) and **N** is the stoichiometric matrix:

$$\begin{pmatrix} 0 & 0 & -1 & 1 & 1 & 1 & -1 & -1 & 0 & 0 & 0 & 0 \\ 0 & 0 & 1 & -1 & 0 & 0 & 0 & 1 & 0 & 0 & 0 & 0 \\ 1 & -1 & -1 & 1 & 0 & 0 & 0 & 0 & 0 & 0 & 0 & 0 \\ -1 & 1 & 0 & 0 & 0 & 0 & 0 & -1 & 0 & 0 & 0 & 0 \\ 0 & 0 & 0 & 0 & -1 & -1 & 1 & 0 & 1 & -1 & 0 & 0 \\ 0 & 0 & 0 & 0 & 0 & 0 & 0 & 0 & -1 & 1 & 1 & -1 \\ 0 & 0 & 0 & 0 & 0 & 0 & 0 & 0 & 0 & 0 & -1 & 1 \\ 0 & 0 & 0 & 0 & 0 & 0 & 0 & 0 & 1 & -1 & 0 & 0 \end{pmatrix}. \tag{4}$$

Each stoichiometric coefficient N_{ij} represents how many molecules of the species S_i have been generated (+ sign) or consumed (- sign) by the reaction v_j. Despite their apparent simplicity, stoichiometric matrices provide valuable information about the reaction networks [21]. Thus, the rank of **N** represents the number of species whose concentrations can be varied independently. For our model with eight variables, $\mathrm{rank}(\mathbf{N}) = 5$ implies the existence of five independent and three dependent variables. The three linear dependences between the species arise from three conservation relationships with simple biochemical meaning:

$$\begin{aligned} &RT + RD + RDI_c + RDI_m + M = \eta^{-1} R_0 \\ &E_c + E_m + M = \eta^{-1} E_0 \\ &I + RDI_m + RDI_c = \eta^{-1} I_0 \end{aligned} \quad , \tag{5}$$

where R_0, I_0, E_0 are the total concentrations of Cdc42, RhoGDI and the Cdc24·Bem1 complex, respectively. As the processes of protein synthesis and degradation can be safely neglected on the time scale of the Cdc42 cluster formation, the total quantities of these species remain constant. We computed the total concentrations as the ratios of the total cellular amounts of the respective species per cytoplasmic volume. Their values are given in the Table S1 together with other model parameters.

In the stationary state $ds/dt = \mathbf{N} \bullet \mathbf{v} = 0$. This implies that the stationary reaction fluxes also obey linear dependences that can be readily obtained from (3):

$$\begin{aligned} &v_1 + v_8 = v_2, \;\; v_3 + v_8 = v_4, \\ &v_5 + v_6 = v_7, \;\; v_9 = v_{10}, \;\; v_{11} = v_{12} \end{aligned} \; . \tag{6}$$

Linear stability analysis of the homogeneous state

We performed a linear analysis of stability for the homogeneous stationary state of model (1) according to the standard procedure as described, e.g., in [22]. This analysis requires calculation of the eigenvalues for the Jacobian matrix of the model equations that had been linearized around the uniform stationary state. Using Matlab, we numerically calculated the eigenvalue λ with the largest real part for the progressively increasing value of the wavenumber *k*. The resulting dispersion curves $\lambda(k)$ are shown in the Figure S1. A positive value of λ at the specific value k_0 indicates that the perturbation with this wavenumber will grow with time, and the uniform stationary state of the model is therefore unstable to any perturbations with the characteristic wavelength $l_0 = 2\pi/k_0$. As we are interested in the emergence of pattern on the closed surface of the plasma

membrane, only certain discrete wavenumbers k_n are allowed. Indeed, any spatio-temporal perturbation of the uniform state can be represented in the form [22]:

$$\mathbf{w}(\mathbf{r},t) = \sum_n c_n e^{\lambda t} \mathbf{W}_n(\mathbf{r}), \tag{7}$$

where $\mathbf{W}_n(\mathbf{r})$ are the eigenfunctions of the diffusion (Laplace's) operator on the chosen surface. For a sphere with radius R, $\mathbf{W}_n(\mathbf{r})$ are the real spherical harmonics Y_n^m [23] with discrete wavenumbers $k_n = \sqrt{n(n+1)}/R$, $n = 0,1,\ldots$, where n represents the number of maxima in the pattern. These functions can be considered as abstract mathematical representation of the elementary patterns with n identical clusters that are positioned on a sphere at the equal distance from each other.

Graph-theoretic analysis of the reaction network

Identification of network elements that are responsible for the particular types of system behavior, e.g., multistability and oscillations, has been an on-going effort for many years [24,25]. Originally developed by B. Clarke [26] and later extended by others [27], the SNA evolved to tackle this problem in the spatially-homogeneous reactions. Recently it has become clear that much the same methods can be used to identify Turing-like instabilities in the spatially-distributed systems with many variables [28,29].

In the framework of the SNA, an arbitrarily complex reaction network can be represented by a bipartite graph (BG) [30] with two types of vertices that represent chemical species and reactions. The vertices of the BG are connected by directed arcs that indicate which species are consumed and produced by the reactions. Eigenvalues λ that define the stability of the reaction network (see above) are the roots of the characteristic polynomial of the system's Jacobian matrix. Only closed subgraphs, or cycles, of the complete BG can destabilize the network since only they contribute negative terms into the coefficients of the characteristic polynomial. Furthermore, a special type of cycles, called "positive", is necessary to destabilize the stationary state of the network. Positive cycles generally correspond to positive feedback loops and often include catalytic reactions. Their formal definition can be found in [30].

Mincheva and Roussel have recently shown that the so-called critical fragments of the BG that contain an odd number of positive cycles may destabilize the stationary state of the spatially-distributed system and cause a Turing-type instability with stationary or oscillatory behavior [31]. To identify potential critical fragments in our network, we first constructed the model BG as shown in the Figure S2. The BG is the graphical representation of the model stoichiometric matrix (4) as can be readily seen from their comparison. The topology of the BG suggests that the reaction network can be subdivided into two modules connected through RD. Due to its simple organization, the

RhoGDI module does not contain elements that can compromise the stability of the network. In contrast, the Cdc42-Bem1-Cdc24 module is replete with positive cycles and includes two catalytic reactions. To aid the graph-theoretic analysis, we also analytically and numerically calculated the coefficients of the characteristic polynomial. Following [31], the elements N_{ij} of the stoichiometric matrix (4) were represented as either $-\alpha_{ij}$, if species *i* is consumed by the reaction *j*, or β_{ij} if species *j* is produced in the reaction *i*. By using this notation for the stoichiometric coefficients instead of their numeric values as in (4) we can match the terms within the coefficients of the characteristic polynomial with the specific network elements in the BG. Further, if the reaction fluxes are formulated according to the mass-action rate law, as in our model, the partial derivatives $\partial v_j / \partial s_i$ that are required for the computation of the Jacobian matrix can be written in the explicit form:

$$\frac{\partial v_j}{\partial s_i} = \alpha_{ij} \frac{v_j}{s_i}. \tag{8}$$

Here v_j and s_i are the values of the respective reaction rate and species concentration that has been calculated for the stationary state under the investigation. Finally, the procedure of Mincheva and Roussel requires that for the analysis of spatially-distributed systems the coefficients of the Jacobian matrix are divided column-wise by the diffusion coefficients of the respective species, e.g., $\tilde{J}_{ij} = J_{ij} / D_j$, where D_j is either D_c or D_m. For our model, the characteristic polynomial can be then represented as:

$$P(\lambda) = \lambda^3 \left(\lambda^5 + p_1 \lambda^4 + p_2 \lambda^3 + p_3 \lambda^2 + p_4 \lambda + p_5 \right), \tag{9}$$

If the spatially uniform steady state loses stability through a non-oscillatory Turing-type mechanism, the coefficient p_5 should become negative, which was confirmed by our numeric and analytic calculations. Two fifth-order critical fragments of the network were identified as responsible for this instability:

$$S_5^1 = \begin{pmatrix} s_1 & s_2 & s_3 & s_5 & s_6 \\ v_8 & v_6 & v_3 & v_{10} & v_{12} \end{pmatrix} \text{ and } S_5^2 = \begin{pmatrix} s_1 & s_2 & s_3 & s_5 & s_6 \\ v_3 & v_6 & v_2 & v_{10} & v_{12} \end{pmatrix}. \tag{10}$$

The principal destabilizing element of the first fragment is the shown in Fig. 3 and highlighted in Fig. S2 positive cycle $C_1 = s_1 \to v_8 \to s_2 \to v_6 \to s_1$. Its topological equivalent, cycle $C_2 = s_1 \to v_3 \to s_2 \to v_6 \to s_1$, comprises the destabilizing influence of the second critical fragment. Our calculations demonstrated that if C_1 is broken by removing reaction v_8, which corresponds to prohibiting binding of the cytoplasmic complex Cdc24·Bem1 to the membrane-bound RT, C_2 alone cannot destabilize the network under any combination of the model parameters. Indeed, from (6) it follows that when $v_8 = 0$, in any stationary state of the model

$$v_3 = v_4 \text{ and } v_7 = v_5 + v_6 . \quad (11)$$

Therefore, the negative contribution of C_2 is always compensated by the positive contribution of the network element that consists of two disjoint edges $(s_2, v_4), (s_1, v_7)$:

$$\frac{v_3 v_6}{s_1 s_2} < \frac{v_4 v_7}{s_1 s_2} . \quad (12)$$

Thus, C_1 is absolutely necessary to destabilize the reaction network shown in Fig. S2 via the non-oscillatory Turing-type route.

Model reduction

To reveal the key species and principal features of the reaction mechanism, we simplified model (1) to the minimal number of equations that describe the formation of the Cdc42 cluster at least qualitatively. In the absence of the standard reduction procedure for an arbitrary reaction-diffusion system, we adopted a number of plausible heuristic assumptions whose domain of validity might be difficult to define strictly. The resulting simplified system should be, thus, considered a reduced version rather then the equivalent of model (1).

First we noted that *in vivo* the fully formed cluster contains only a small proportion of the full cellular Cdc42 store (~3% according to [32]) and thus the most of Cdc42 remains in the RDI form. The cluster emerges from the uniform stationary state (USS) through a redistribution of the RT on the membrane rather than transfer of additional RD from the cytoplasm. Therefore we posited that the concentration of the free GDI in the cytoplasm, *I*, remains approximately constant throughout the cluster formation and its spatial variation is negligible. We set $I = I_0$, the concentration of I in the USS. We also assumed that the spatial variation of E_c, the cytoplasmic Cdc24·Bem1 complex, can be neglected and E_c can be found from the mass conservation relation (5):

$$E_c = E_c^0 - \int_S (M + E_m)\ dS , \quad (13)$$

where $E_c^0 = \eta^{-1} E_0$ and the integral is taken over the entire membrane surface *S*.

We also noted that, throughout the cluster formation, variables of model (1) reach their stationary values with different kinetics, with RT and RD being the slowest variables. Assuming that the kinetics of the membrane variables is predominantly defined by the local reaction rather then diffusion, we reduced the number of model variables by applying the standard quasi steady-state approximation to the fast variables. Assuming $dM/dt = 0$ and $dE_m/dt = 0$, we obtained:

$$E_m = E_c\left(\frac{k_1}{k_{-1}} + \frac{k_7}{k_{-1}}RT\right),\ M = E_c \cdot RT\left(\frac{k_4 k_7}{k_{-4}k_{-1}}RT + \frac{k_4 k_1}{k_{-4}k_{-1}} + \frac{k_7}{k_{-4}}\right). \quad (14)$$

Noting that $k_2 E_m \ll k_3 M$, the equation for RT can be simplified further:

$$\frac{\partial RT}{\partial t} = k_3 M \cdot RD - k_{-2}RT + D_m \Delta RT. \quad (15)$$

Substituting (14) into (15) we got:

$$\frac{\partial RT}{\partial t} = k_3 E_c \cdot RT\left(\frac{k_4 k_7}{k_{-4}k_{-1}}RT + \frac{k_4 k_1}{k_{-4}k_{-1}} + \frac{k_7}{k_{-4}}\right) \cdot RD - k_{-2}RT + D_m \Delta RT. \quad (16)$$

Applying quasi steady-state approximation $dRDI_m/dt = 0$ we also found

$$RDI_m = \frac{k_6 I_0}{k_{-6} + k_{-5}}RD + \frac{k_5}{k_{-6} + k_{-5}}RDI_c. \quad (17)$$

To achieve further reduction of the model, we adopted the approach based on the following observation. The membrane-bound RD is at all times in a fast equilibrium with its cytoplasmic form RDI. The ability to perform frequent membrane-cytoplasmic transitions enables the molecules of RD to propagate along the membrane in a series of adsorption-desorption events with the effective diffusion coefficient $D_{mc} \gg D_m$. This biophysical phenomenon can be readily demonstrated using the rapid buffering approximation (RBA) originally developed by Wagner and Keiser for the diffusion of Ca^{2+} in the cytoplasm [33]. Recently the RBA was adopted by Jilkine *et al*. for the membrane-cytoplasmic transport [34]. To apply RBA to our system, we first introduced a new variable that describes the total concentration of the inactive form of Cdc42 on the membrane and in the adjacent cytoplasm $RD_{tot} = RD + RDI_c$. Adding the equations for RD and RDI_c we obtained the equation for the new variable:

$$\frac{\partial}{\partial t}\left(RD + RDI_c\right) = \frac{\partial RD_{tot}}{\partial t} = k_{-2}RT - k_3 M(RT, E_c) \cdot RD + D_m \Delta RD + D_c \Delta RDI_c. \quad (18)$$

Using (17) and the RBA assumption of fast equilibrium between RD and RDI_c, we got $k_6 I_0 k_{-5} RD = k_{-6} k_5 RDI_c$. From this, RD and RDI_c can be expressed through RD_{tot} as follows:

$$RD = RD_{tot}\left(\frac{k_5/k_{-5}}{k_5/k_{-5} + I_0 \cdot k_6/k_{-6}}\right),\ RDI_c = RD_{tot}\left(\frac{I_0 \cdot k_6/k_{-6}}{k_5/k_{-5} + I_0 \cdot k_6/k_{-6}}\right). \quad (19)$$

Substituting (19) into (18) we obtained:

$$\frac{\partial RD_{tot}}{\partial t} = k_{-2}RT - k_3 M(RT, E_c)\cdot RD_{tot}\left(1+\zeta\right)^{-1} + D_{mc}\Delta RD_{tot}, \tag{20}$$

where $D_{mc} = D_m\left(1+\zeta\right)^{-1} + D_c\zeta\left(1+\zeta\right)^{-1}$ and $\zeta = I_0 \cdot k_6 k_{-5}/k_{-6}k_5$. Given the values of the model parameters, $\zeta \gg 1$ and, therefore $D_{mc} \approx D_c$. Finally, assembling equations (13), (16) and (20) we obtained the reduced model:

$$\begin{aligned}
&\frac{\partial RT}{\partial t} = \alpha E_c \cdot RT^2 \cdot RD + \beta E_c \cdot RT \cdot RD - \gamma RT + D_m \Delta RT,\\
&\frac{\partial RD_{tot}}{\partial t} = \gamma RT - \alpha E_c \cdot RT^2 \cdot RD - \beta E_c \cdot RT \cdot RD + D_c \Delta RD_{tot},\\
&E_c = E_c^0 \Bigg/ \left(1 + \int_S dS\left[RT^2\left(\frac{k_4 k_7}{k_{-4}k_{-1}}\right) + RT\left(\frac{k_4 k_1 + k_7 k_{-1} + k_7 k_{-4}}{k_{-4}k_{-1}}\right) + \frac{k_1}{k_{-1}}\right]\right).
\end{aligned} \tag{21}$$

To simplify the form of these equations, we introduced the following notations:

$$\alpha = k_3\frac{k_4 k_7}{k_{-4}k_{-1}}(1+\zeta)^{-1},\ \ \beta = k_3\left(\frac{k_4 k_1}{k_{-4}k_{-1}} + \frac{k_7}{k_{-4}}\right)(1+\zeta)^{-1},\ \ \gamma = k_{-2}.$$

Due to the conservation of the total amount of cellular Cdc42, the reaction terms in the equations for RT and RD_{tot} in model (21) exactly compensate each other. Equations of this general type have been recently brought to the attention by Otsuji *et al*. [35] as capable of describing spatial structure in the systems with mass conservation. The last equation in (21) represents conservation of total E_c and is not required for the emergence of structure in model (21). Neglecting E_c conservation, however, results in the conversion of the entire cellular Cdc42 into the cluster, which apparently contradicts the experimental data. Using numeric simulations, we confirmed that system (21) generates spatial structure that qualitatively recapitulates all features of the Cdc42 cluster observed in the complete model (1).

Supplementary Movie S1. Formation of the unique Cdc42 cluster in the simulation with stochastic activation of Cdc42 on the membrane in the absence of landmark proteins. The stationary cluster emerges through the competition of two cluster nuclei clearly resolved in the sequence. The concentration of RT is color-coded as in Figure 2.

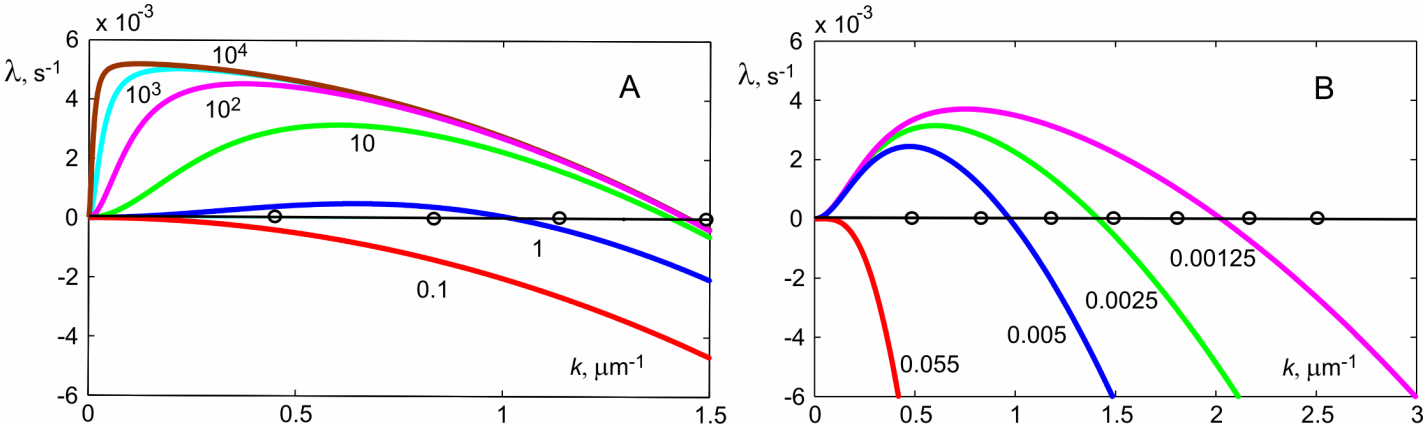

Figure S1. Spatially uniform stationary state of the model is unstable to perturbations with finite wavelength as demonstrated here by the linear analysis of stability (see Methods). A – Dispersion curves for $D_m = 0.0025 \mu m^{-2}/s$ and the indicated on the figure values of D_c. The range of unstable wavenumbers shrinks as the cytoplasmic diffusion coefficient D_c is decreased and disappears altogether below the critical value $D_c^* = 0.1 \mu m^{-2}/s$. In contrast, the increase of D_c beyond the value $D_c = 10 \mu m^{-2}/s$, an estimate for the medium-sized proteins, does not further widen the range of unstable wave numbers. B - Dispersion curves for $D_c = 10 \mu m^{-2}/s$ and the indicated values of D_m. Reduction of the membrane diffusion coefficient progressively increases the range of unstable wave numbers. Discrete wavenumbers $k_n = \sqrt{n(n+1)}/R,\ n = 0,1,\ldots$ for the real spherical harmonic functions with progressively increasing number of maxima n are shown by circles on the x axis. The values of k_n are computed for spherical cell with $R = 3 \mu m$.

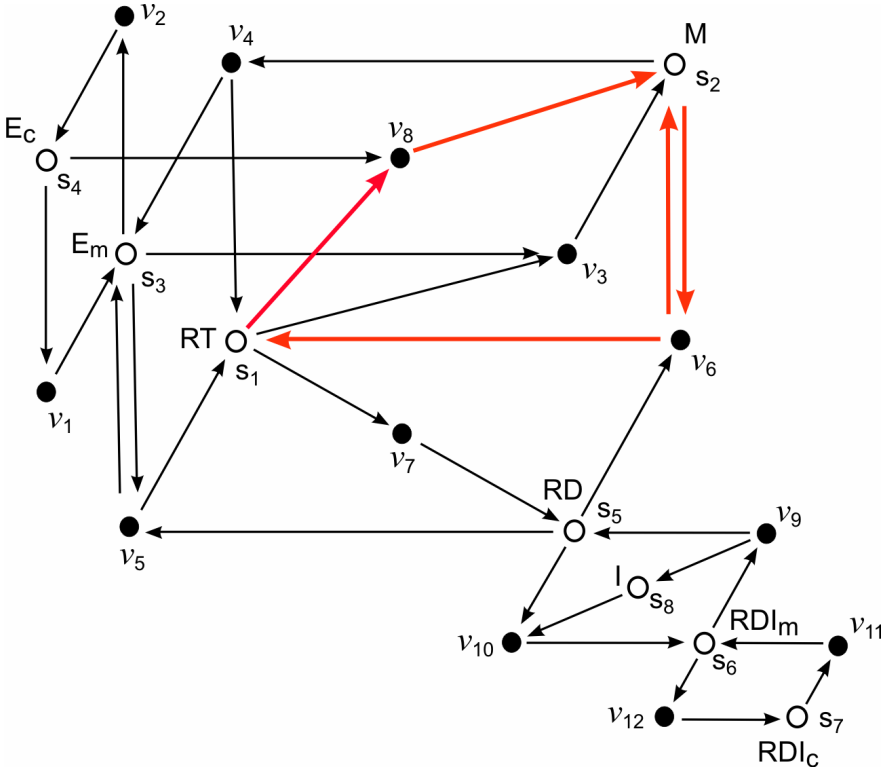

Figure S2. The reaction network of model (1) is represented by a bipartite graph. Two types of nodes, molecular species and reactions are shown by open and filled circles, respectively. Directed edges of the graph represent the flow of the reaction fluxes. The edges shown by double arrows with opposite directions represent catalysis and, thus, no mass flow occurs through these edges. The autocatalytic cycle (see Fig. 3) that destabilizes the uniform stationary state of the network is highlighted in red.

Table S1. Reaction rate constants and parameters of the model.

Constant	Value	Reference
k_1	10 s^{-1}	[36-39]
k_{-1}	10 s^{-1}	[40]
k_2	0.0001 $\mu M^{-1} \cdot s^{-1}$	[10]
$k_{-2,1}$ / $k_{-2,0}$	0.017 $\mu M^{-1} \cdot s^{-1}$/ 0.00033 s^{-1}	[10]
k_3	0.01 $\mu M^{-1} \cdot s^{-1}$	[10]
k_4	10 $\mu M^{-1} \cdot s^{-1}$	[10]
k_{-4}	0.3 s^{-1}	[10]
k_5	0.9 s^{-1}	[4]
k_{-5}	0.13 s^{-1}	[5]
k_6	1.5 $\mu M^{-1} \cdot s^{-1}$	[5]
k_{-6}	0.5 s^{-1}	[5]
k_7	10 $\mu M^{-1} \cdot s^{-1}$	[10]
R_0	5 μM	[3]
A_0	1 μM	[6,41]
E_0	0.017 μM	[41]

Table S2. The stationary Cdc42 cluster is robust to variation of the model parameters. The relative change in the cluster maximal RT concentration (the upper cell value) and the cluster width* (the lower cell value) were computed for the model parameter values given in the Table S1 multiplied by the factors shown in the head row of the table. Reaction rate k_2 is not reported since its effect on the stationary state of the model is quantitatively negligible. The cluster was found to have identical zero sensitivity to the variation of k_1 and k_7 while their change was exactly compensated by the change in the stationary concentration of E_c.

Reaction rate constant	× 2	× 0.5
k_1	0 0	0 0
k_{-1}	+0.20 -0.07	-0.20 +0.13
k_{-2}	-0.20 -0.17	+0.17 +0.13
k_3	+0.35 +0.9	-0.31 -0.13
k_4	-0.20 +0.15	+0.20 -0.13
k_{-4}	+0.21 -0.13	-0.20 +0.13
k_5	+0.28 0	-0.01 0
k_{-5}	-0.20 -0.09	+0.21 +0.04
k_6	-0.20 -0.09	+0.23 +0.04
k_{-6}	+0.24 +0.04	-0.20 -0.09
k_7	0 0	0 0

***** The width of the RT concentration profile in the cluster was measured as the distance between the points where the net membrane-cytoplasmic flux of RD changes sign.

References

[1] Irazoqui, J.E., Gladfelter, A.S. and Lew, D.J. (2003) Scaffold-mediated symmetry breaking by Cdc42p. Nat. Cell Biol. 5**,** 1062-1070.

[2] Shimada, Y., Wiget, P., Gulli, M.P., Bi, E. and Peter, M. (2004) The nucleotide exchange factor Cdc24p may be regulated by auto-inhibition. EMBO J. 23**,** 1051-1062.

[3] Michaelson, D., Silletti, J., Murphy, G., D'Eustachio, P., Rush, M. and Philips, M.R. (2001) Differential localization of Rho GTPases in live cells: regulation by hypervariable regions and RhoGDI binding. J. Cell Biol. 152**,** 111-126.

[4] Robbe, K., Otto-Bruc, A., Chardin, P. and Antonny, B. (2003) Dissociation of GDP dissociation inhibitor and membrane translocation are required for efficient activation of Rac by the Dbl homology-pleckstrin homology region of Tiam. J. Biol. Chem. 278**,** 4756-4762.

[5] Nomanbhoy, T.K., Erickson, J.W. and Cerione, R.A. (1999) Kinetics of Cdc42 membrane extraction by Rho-GDI monitored by real-time fluorescence resonance energy transfer. Biochemistry 38**,** 1744-1750.

[6] Smith, G.R., Givan, S.A., Cullen, P. and Sprague, G.F., Jr. (2002) GTPase-activating proteins for Cdc42. Eukaryot. Cell 1**,** 469-480.

[7] Terasawa, H., Noda, Y., Ito, T., Hatanaka, H., Ichikawa, S., Ogura, K., Sumimoto, H. and Inagaki, F. (2001) Structure and ligand recognition of the PB1 domain: a novel protein module binding to the PC motif. EMBO J. 20**,** 3947-3956.

[8] Zheng, Y., Bender, A. and Cerione, R.A. (1995) Interactions among proteins involved in bud-site selection and bud-site assembly in Saccharomyces cerevisiae. J. Biol. Chem. 270**,** 626-630.

[9] Gulli, M.P., Jaquenoud, M., Shimada, Y., Niederhauser, G., Wiget, P. and Peter, M. (2000) Phosphorylation of the Cdc42 exchange factor Cdc24 by the PAK-like kinase Cla4 may regulate polarized growth in yeast. Mol. Cell 6**,** 1155-1167.

[10] Goryachev, A.B. and Pokhilko, A.V. (2006) Computational model explains high activity and rapid cycling of Rho GTPases within protein complexes. PLoS. Comput. Biol. 2**,** e172.

[11] Grosshans, B.L., Ortiz, D. and Novick, P. (2006) Rabs and their effectors: achieving specificity in membrane traffic. Proc. Natl. Acad. Sci. U. S. A 103**,** 11821-11827.

[12] Lippe, R., Miaczynska, M., Rybin, V., Runge, A. and Zerial, M. (2001) Functional synergy between Rab5 effector Rabaptin-5 and exchange factor Rabex-5 when physically associated in a complex. Mol. Biol. Cell 12**,** 2219-2228.

[13] Hussain, N.K., Jenna, S., Glogauer, M., Quinn, C.C., Wasiak, S., Guipponi, M., Antonarakis, S.E., Kay, B.K., Stossel, T.P., Lamarche-Vane, N. and McPherson, P.S. (2001) Endocytic protein intersectin-l regulates actin assembly via Cdc42 and N-WASP. Nat. Cell Biol. 3**,** 927-932.

[14] Kholodenko, B.N., Hoek, J.B. and Westerhoff, H.V. (2000) Why cytoplasmic signalling proteins should be recruited to cell membranes. Trends Cell Biol. 10**,** 173-178.

[15] Markevich, N.I., Moehren, G., Demin, O.V., Kiyatkin, A., Hoek, J.B. and Kholodenko, B.N. (2004) Signal processing at the Ras circuit: what shapes Ras activation patterns? Syst. Biol. (Stevenage.) 1**,** 104-113.

[16] Brown, G.C. and Kholodenko, B.N. (1999) Spatial gradients of cellular phospho-proteins. FEBS Lett. 457**,** 452-454.

[17] Valdez-Taubas, J. and Pelham, H.R. (2003) Slow diffusion of proteins in the yeast plasma membrane allows polarity to be maintained by endocytic cycling. Curr. Biol. 13**,** 1636-1640.

[18] Greenberg, M.L. and Axelrod, D. (1993) Anomalously slow mobility of fluorescent lipid probes in the plasma membrane of the yeast Saccharomyces cerevisiae. J. Membr. Biol. 131**,** 115-127.

[19] Schaff, J., Fink, C.C., Slepchenko, B., Carson, J.H. and Loew, L.M. (1997) A general computational framework for modeling cellular structure and function. Biophys. J. 73**,** 1135-1146.

[20] Gomatam, J. and Amdjadi, F. (1997) Reaction-diffusion equations on a sphere: Meandering of spiral waves. Phys. Rev. E 56**,** 3913-3919.

[21] Hofmeyr, J.H., Snoep, J. and Westerhoff, H.V. (2002) Kinetics, control and regulation of metabolic systems. ICSB 2002 Tutorial.

[22] Murray, J.D. (1993) Mathematical biology, 2nd, Corrected Edition. Springer-Verlag, New York.

[23] Korn, G.A. and Korn, T.M. (1968) Mathematical handbook for scientists and engineers. McGraw-Hill, New York.

[24] Tyson, J.J. (1975) Classification of instabilites in chemical reaction systems. J. Chem. Phys. 62**,** 1010-1015.

[25] Feinberg, M. (1987) Chemical- reaction network structure and the stability of complex isothermal reactors.1. The deficiency- zero and deficiency- one theorems. Chem. Eng. Sci. 42**,** 2229-2268.

[26] Clarke, B.L. (1988) Stoichiometric network analysis. Cell Biophys. 12**,** 237-253.

[27] Ivanova, A.N. (1979) Conditions for uniqueness of the stationary states of kinetic systems, connected with the structures of their reaction- mechanisms .1. Kinetics and Catalysis 20**,** 833-837.

[28] Satnoianu, R.A., Menzinger, M. and Maini, P.K. (2000) Turing instabilities in general systems. J. Math. Biol. 41**,** 493-512.

[29] Qian, H. and Murray, J.D. (2001) A simple method of parameter space determination for diffusion-driven instability with three species. Appl. Math. Lett. 14**,** 405-411.

[30] Mincheva, M. and Roussel, M.R. (2007) Graph-theoretic methods for the analysis of chemical and biochemical networks. I. Multistability and oscillations in ordinary differential equation models. J. Math. Biol. 55**,** 61-86.

[31] Mincheva, M. and Roussel, M.R. (2006) A graph-theoretic method for detecting potential Turing bifurcations. J. Chem. Phys. 125**,** 204102.

[32] Wedlich-Soldner, R., Wai, S.C., Schmidt, T. and Li, R. (2004) Robust cell polarity is a dynamic state established by coupling transport and GTPase signaling. J. Cell Biol. 166**,** 889-900.

[33] Wagner, J. and Keizer, J. (1994) Effects of rapid buffers on Ca2+ diffusion and Ca2+ oscillations. Biophys. J. 67**,** 447-456.

[34] Jilkine, A., Maree, A.F. and Edelstein-Keshet, L. (2007) Mathematical Model for Spatial Segregation of the Rho-Family GTPases Based on Inhibitory Crosstalk. Bull. Math. Biol. 69**,** 1943-1978.

[35] Otsuji, M., Ishihara, S., Co, C., Kaibuchi, K., Mochizuki, A. and Kuroda, S. (2007) A Mass Conserved Reaction-Diffusion System Captures Properties of Cell Polarity. PLoS. Comput. Biol. 3**,** e108.

[36] Ago, T., Takeya, R., Hiroaki, H., Kuribayashi, F., Ito, T., Kohda, D. and Sumimoto, H. (2001) The PX domain as a novel phosphoinositide- binding module. Biochem. Biophys. Res. Commun. 287**,** 733-738.

[37] Dove, S.K., Cooke, F.T., Douglas, M.R., Sayers, L.G., Parker, P.J. and Michell, R.H. (1997) Osmotic stress activates phosphatidylinositol-3,5-bisphosphate synthesis. Nature 390**,** 187-192.

[38] Mitra, P., Zhang, Y., Rameh, L.E., Ivshina, M.P., McCollum, D., Nunnari, J.J., Hendricks, G.M., Kerr, M.L., Field, S.J., Cantley, L.C. and Ross, A.H. (2004) A novel phosphatidylinositol(3,4,5)P3 pathway in fission yeast. J. Cell Biol. 166**,** 205-211.

[39] Snyder, J.T., Rossman, K.L., Baumeister, M.A., Pruitt, W.M., Siderovski, D.P., Der, C.J., Lemmon, M.A. and Sondek, J. (2001) Quantitative analysis of the effect of phosphoinositide interactions on the function of Dbl family proteins. J. Biol. Chem. 276**,** 45868-45875.

[40] Yu, J.W. and Lemmon, M.A. (2001) All phox homology (PX) domains from Saccharomyces cerevisiae specifically recognize phosphatidylinositol 3-phosphate. J. Biol. Chem. 276**,** 44179-44184.

[41] Ghaemmaghami, S., Huh, W.K., Bower, K., Howson, R.W., Belle, A., Dephoure, N., O'Shea, E.K. and Weissman, J.S. (2003) Global analysis of protein expression in yeast. Nature 425**,** 737-741.